Role of measurement uncertainties in observed variability in the spectral backscattering ratio: a case study in mineral-rich coastal waters

David McKee,[1,*] Malik Chami,[2] Ian Brown,[1] Violeta Sanjuan Calzado,[3] David Doxaran,[2] and Alex Cunningham[1]

[1]Physics Department, University of Strathclyde, 107 Rottenrow, Glasgow, G4 ONG, Scotland

[2]Laboratoire d'Océanographie de Villefranche, Université Pierre et Marie Curie–Paris 6, Unité Mixte de Recherche CNRS 7093, BP 28, F-06234 Villefranche-sur-Mer Cedex, France

[3]National Oceanography Centre Southampton, University of Southampton, Waterfront Campus, European Way, Southampton SO14 3ZH, United Kingdom

*Corresponding author: david.mckee@strath.ac.uk

Received 24 November 2008; revised 22 July 2009; accepted 23 July 2009; posted 23 July 2009 (Doc. ID 104504); published 11 August 2009

The particulate backscattering ratio (b_{bp}/b_p) is a useful indicator of the angular scattering characteristics of natural waters. Recent studies have shown evidence both for and against significant spectral variability in b_{bp}/b_p in the visible domain, but most show significant variability in its magnitude. We present results from a case study in which both backscattering and scattering coefficients were measured at nine wavelengths in a region of UK coastal waters where optical scattering is strongly influenced by inorganic particles and where a wide range of turbidities is found in a small geographic area. Using a new approach based on regression analysis of *in situ* signals, it is shown that, for this study site, most of the apparent variability in the magnitude of the backscattering ratio can be attributed to measurement uncertainties. Regression analysis suggests that b_{bp}/b_p is wavelength dependent for these mineral-rich waters. This conclusion can only be avoided by positing the existence of undocumented, systematic, wavelength-dependent errors in backscattering measurements made by two independently calibrated sensors. These results are important for radiative transfer simulations in mineral-dominated waters where the backscattering ratio has often been assumed to be spectrally flat. Furthermore, spectral dependence also has profound implications for our understanding of the relationship between b_{bp}/b_p and particle size distributions in coastal waters since the commonly assumed power-law distribution is associated with a spectrally flat particulate backscattering ratio for nonabsorbing particles.

OCIS codes: 010.4450, 010.4458, 010.1350.

1. Introduction

The radiative transfer equation, which describes the propagation of photons through natural waters, requires knowledge of both the absorption and the angular scattering characteristics of the medium. Despite recent advances, *in situ* measurements of the volume scattering function (VSF) over the full range of scattering angles are technically demanding and remain relatively scarce [1–4]. It has been shown, however, that the scattering phase function can be reasonably approximated from the backscattering ratio [5]. A new generation of commercial *in situ* sensors has been developed that provides measurements of the required optical parameters:

0003-6935/09/244663-13$15.00/0

the coefficients of absorption, attenuation, and backscattering (with scattering obtained by subtraction of absorption from attenuation). These sensors have been deployed in a wide variety of natural waters across the globe and large data sets now appear in the literature [6–8].

An understanding of systematic and random measurement uncertainties is required prior to analysis of the measured optical properties. For example, any measurement of an inherent optical property (IOP), such as absorption, is likely to be subject to systematic error due to incomplete accounting for scattering collection error [9–12]. Other IOPs are derived from measurements that require assumptions about the shape of the VSF that may not be universally applicable [13]. Furthermore, each instrument will have a characteristic noise level that introduces a degree of random uncertainty. For parameters such as the backscattering ratio, where combinations of measurements are involved, the random uncertainty is potentially further enhanced by inhomogeneity of material distributions on small physical scales and the fact that each contributing measurement is not made on exactly the same sample of water [14]. Furthermore, pumped flow-through instruments (such as the WETLabs AC9) could be affected by disruption of aggregates of particles, while backscattering sensors are much less likely to disturb the particle population in this manner.

The backscattering ratio is a particularly important parameter as it is widely used as a proxy to determine scattering phase functions [5]. The particulate backscattering ratio (b_{bp}/b_p) may also be useful as a proxy for particle composition as it can be related to particle size distribution (PSD) and refractive index [15]. Theoretical studies have suggested that the particulate backscattering ratio should be wavelength independent if the particles are not strongly pigmented, and the particle size distribution follows the commonly assumed power-law distribution [16]. However, it has been shown that pigmented particles following a power-law size distribution would have a spectrally variable backscattering ratio through the influence of the imaginary component of the refractive index [17,18]. The literature contains conflicting views on whether field measurements support a wavelength-dependent backscattering ratio. Studies in coastal waters have found evidence for wavelength-dependent scattering phase functions [4,7,10,19], while other studies with more open ocean stations suggest that b_{bp}/b_p is wavelength independent [8,18]. There are a number of reasons why it is important that these differing views are resolved. For example, the widely used scattering correction procedure for AC9 absorption measurements proposed by Zaneveld *et al.* [20] is based on an assumption of a wavelength-independent scattering phase function. Models of underwater light fields for remote sensing and primary productivity studies are also dependent on assumptions about the nature of the scattering phase function.

This study examines the role of measurement uncertainty in the determination of b_{bp}/b_p. Although attempts have already been made to quantify instrument uncertainties, a new approach was adopted using the analysis of *in situ* signals. The aim is to develop an understanding of observed variability in particulate backscattering ratios derived from *in situ* IOP measurements and to establish a robust method for determining the wavelength variability of b_{bp}/b_p. Data are considered both as individual sets of measurements for each location and depth, and as an assemblage of observations representative of the optical properties of the region.

2. Methods

A. Optical Measurements

Absorption (a_n) and attenuation (c_n) coefficients for non-water materials were measured at nine wavelengths (412, 440, 488, 510, 532, 555, 650, 676, and 715 nm) in the visible–NIR with a WETLabs AC9 calibrated with Milli-Q ultrapure water. Absorption was corrected for scattering effects using the method of Zaneveld *et al.* [20]. This method was used for consistency with other data sets, but it is based on assumptions of wavelength independence for the scattering phase function and zero absorption at 715 nm, which may not hold for the waters sampled [10,21]. Data were corrected for temperature and salinity effects using the coefficients of Sullivan *et al.* [22] and data from a SeaBird SBE19-Plus CTD (conductivity, temperature, and depth) instrument. Particulate scattering (b_p) was obtained from $b_p = c_n - a_n$. Visible–NIR particulate backscattering was determined from VSF measurements made with a WETLabs ECO-BB9 (412, 440, 488, 510, 532, 595, 660, 676, and 715 nm). The instrument was calibrated by the manufacturer prior to shipping shortly before the cruise, and data were corrected for path-length absorption effects using the correction factor provided by the manufacturer. The conversion from VSF to b_{bp} was performed using the χ_p factor from Boss and Pegau [23], though we note that this is subject to some variability [13]. The AC9 and BB9 did not have completely matched wavelengths, and data were interpolated to give b_{bp} at 555 and 650 nm. All data were averaged into 1 m depth bins. The number of samples varies between 572 and 742 data points, according to wave band, as the BB9 sensor saturates at different backscattering levels for each channel. A HOBI Labs Hydroscat-2 was used at a subsample of stations (334 data points per channel) to provide backscattering data at 470 and 676 nm. Hydroscat-2 data were corrected for path-length absorption effects using coefficients provided by the manufacturer. AC9 data were linearly interpolated to provide b_p to match Hydroscat-2 b_{bp} at 470 nm. The Hydroscat-2 676 nm channel has a 20 nm FWHM filter to permit dual use as a

chlorophyll fluorometer. There is, therefore, potential for fluorescence contamination of this channel. However, it should be noted that the signal was dominated by mineral backscattering in this region and that the effect of any fluorescence contamination would be to increase the apparent backscattering at this wavelength. Correction for fluorescence effects on the 676 nm Hydroscat-2 backscattering channel would, therefore, enhance any observed wavelength dependency in the backscattering ratio.

The WETLabs BB9 and HOBI Labs Hydroscat-2 sensors have different optical geometries, though both make wide angle measurements of volume scattering that require extrapolation to give b_{bp}. They are calibrated using quite different methodologies. The BB9 is calibrated using polystyrene microspheres in a series of dilutions, with Mie theory used to calculate volume scattering function values for each set of dilutions. This calibration method requires knowledge of the scattering collection geometry and wavelength bandwidth for each optical channel, the refractive index and size distribution of the beads, and a method to normalize measurements to the total scattering coefficient (currently realized by making simultaneous measurements of attenuation with a WETLabs AC9). Each of these aspects of the manufacturer's calibration procedure carries an associated uncertainty that is currently difficult to quantify. The Hydroscat-2 is calibrated by measuring the scattered signal from a submerged reflectance target that traverses the scattering volume of the sensor [24]. Here the reflectance of the target is critical in determining the uncertainty in the calibration. In both cases, the purpose of the calibration exercise is to determine the calibration slope that relates the measured signal (minus a dark signal) to the VSF corresponding to the sensor optical geometry. Whitmire *et al.* [8] provided a detailed analysis of the likely errors affecting Hydroscat and AC9 calibration and reached the conclusion that the likely maximum error in b_{bp}/b_p would be around 20%. Their estimate erred on the side of caution in the propagation of errors and was greater than the ~10% differences in b_{bp}/b_p found in comparisons made among different instruments and methods [14]. The present study focuses primarily on the effect of other measurement uncertainties, such as limitations in the performance of the AC9 scattering correction and random uncertainties due to different sensors not measuring the same sample volume. However, uncertainty in the calibration slope is clearly a serious issue, particularly when discussing observations of spectral variability in b_{bp}/b_p.

B. Sample Analyses

Chlorophyll samples were filtered through 25 mm GF/F filters and immediately frozen. Once in the laboratory, the filter papers were soaked for 24 h in neutralized 90% acetone, and the absorbance of the extract measured in a Shimadzu UV-2501PC spectrophotometer using 1 cm path-length cuvettes before and after acidification with dilute hydrochloric acid. The trichromatic equations of Jeffrey and Humphrey [25] were used to convert absorbance spectra to concentrations of chlorophyll *a* (Chl). All samples were measured in triplicate. Total suspended solids (TSS) samples were obtained by filtering 5 liters of seawater through preweighed 90 mm GF/F filters and rinsing with 50 ml of distilled water. Samples were stored frozen until returned to the laboratory, where they were dried in an oven at 100 °C for 3 h and reweighed. The concentration of mineral suspended solids (MSS) was obtained by reweighing samples after they had been placed in a furnace at 500 °C for 3 h, at which point it was assumed that all organic materials had been combusted. Colored dissolved organic materials (CDOM) samples were filtered through 0.2 μm membrane filters, with the filtrate being collected in acid-rinsed glass bottles with Nalgene caps and stored under refrigeration. Absorption by CDOM was measured in the Shimadzu UV-2501PC spectrophotometer using 10 cm cuvettes and UV treated ultrapure water as a reference. Given the unknown and probably complex chemical composition of CDOM, the absorption coefficient of the filtrate material at 440 nm was used as a proxy for the concentration of CDOM.

3. Results and Discussion

A. Location of Experiment

Previous studies have presented data from a wide range of water types. Indeed, one study claims to be representative of the global ocean [8]. There are two issues with this approach. The first is the underlying assumption that a global trend exists that can be exposed by sampling enough points. There is no reason to suppose that there is a globally relevant b_{bp}/b_p anymore than there is an equivalently global specific absorption coefficient. The second issue is the difficulty in identifying local trends and relationships in the midst of very large data sets. In this study we examine data from a single cruise in the Bristol Channel (Fig. 1). This shallow, macrotidal estuary experiences very strong resuspension of sediment, giving a broad range of scattering signals within a limited geographic range. The mineral component of total suspended particulate material (MSS) reached concentrations as high as 15 g m^{-3} for the optical data presented here (at which point all of the BB9 optical channels were saturated), corresponding to a median value of 82% of the total suspended particulate material. The maximum Chl concentration was less than 3.5 mg m^{-3} with a median value of 1.25 mg m^{-3}. Figure 2 shows all the absorption, attenuation, scattering, and backscattering spectra obtained for this study. Figure 2(d) illustrates the manner in which each backscattering channel reached saturation at different levels of turbidity, with blue-green channels able to operate over considerably greater dynamic ranges than red-NIR channels. Figures 2(b) and 2(c) show attenuation

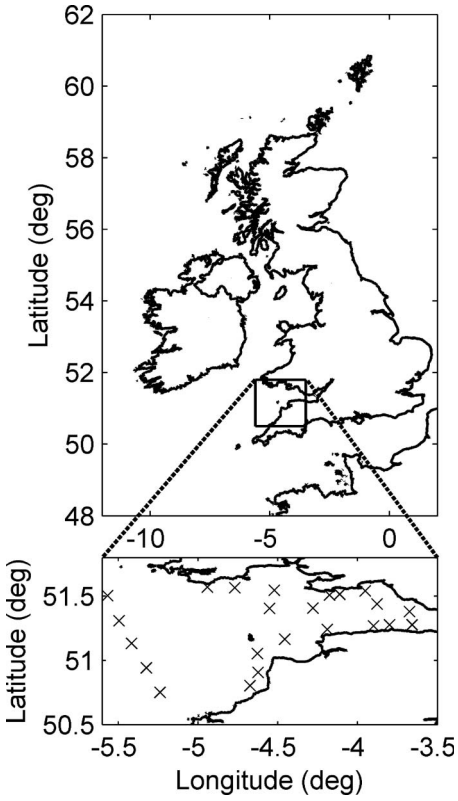

Fig. 1. Map of the British Isles with the location of the sampling area in the Bristol Channel marked with a rectangle. The lower panel shows station positions in the Bristol Channel marked by crosses.

and particulate scattering spectra with consistent spectral shapes across the full range of observations. Absorption spectra [Fig. 2(a)] show strong increases toward blue wavelengths, consistent with strong contributions from mineral particles and/or CDOM. There are also significant absorption peaks at 676 nm for some of the samples, suggesting an influence of phytoplankton on red absorption values. In this study we are primarily interested in particulate scattering and backscattering, and it is necessary to assess to what extent these parameters are influenced by either MSS or Chl. Coefficients of determination obtained by linear regression of b_{bp}, b_p, and a_n against MSS and Chl are given in Table 1. MSS accounts for between 65% and 87% of observed variability in b_{bp}, with lower values in the red-NIR due to reduced dynamic range at these wavelengths as a result of sensor saturation. MSS accounts for ~85% of observed variability in b_p for all wavelengths. The influence of Chl on either b_{bp} or b_p is minimal across the data set, with maximum values of 5% for red-NIR b_{bp} and <1% for all other b_{bp} and b_p. MSS also accounts for 85% of observed variability in a_n, with the exception of 676 nm, where it only accounts for 65% of the variability. Chlorophyll accounts for 31% of variability in a_n at 676 nm, 5% at 650 nm, and is elsewhere insignificant (<1% observed variability). The median absorption by CDOM at 440 nm was 0.16 m^{-1} with a maximum value of 0.50 m^{-1}. Over the entire data set, CDOM absorption only accounted for ~7% of the observed variability in non-water absorption at 440 nm. From this we can conclude that IOPs in the Bristol Channel are strongly influenced by mineral particles, although there are instances where absorption at 676 nm is obviously affected by algal pigments. The fact that particulate scattering and backscattering are dominated by a population of nonbiogenic mineral particles is important in this context as it reduces the complexity of the data set for subsequent analysis, and we can anticipate that there ought to be less variability in b_{bp}/b_p than would be observed in a data set covering waters with a wide variety of particle composition. Of course, there may remain instances in the data set, particularly specific locations and/or depths where MSS is low, where phytoplankton may have a significant influence on b_p or b_{bp}, but we have demonstrated that, when we treat these parameters as an assemblage representative of the region, the influence of MSS is dominant.

B. Statistical Approaches

In this study we analyze variability in the particulate backscattering ratio using two different approaches. The first is a point-by-point method where individual measurements of particle backscattering, b_{bp}, are divided by corresponding individual measurements of particle scattering, b_p, and variability is assessed using descriptive statistics of the resulting distributions of particulate backscattering ratio, b_{bp}/b_p. The second approach uses linear regression to find best-fit values of b_{bp}/b_p for the data set as a whole.

C. b_{bp}/b_p from a Point-by-Point Approach

Figure 3 shows the distribution of particulate backscattering ratios calculated from individual measurements of b_p and b_{bp} for this data set. The 532 nm channel has been selected as generally representative of the distributions found for all the measured wavelengths. b_{bp}/b_p appears to vary over an order of magnitude with values ranging from 0.0065 to 0.0675, a mean value of 0.031, and a median value of 0.029. This is a very broad range, even greater than that presented by Whitmire *et al.* for the global ocean [8], and is most surprising given the restricted geographic range of the sample locations. If these data were taken at face value, they would suggest marked variability in material composition, particle size distribution, or both. Of course, it is also necessary to consider other potential sources of apparent variability, including measurement uncertainties.

D. b_{bp}/b_p from a Regression Approach

The backscattering and scattering values used to generate the distribution of b_{bp}/b_p shown in Fig. 3 are plotted against each other in Fig. 4. As there is measurement uncertainty in both x and y variables, geometric mean regression was used to determine the best-fit line through the data. The best-fit line

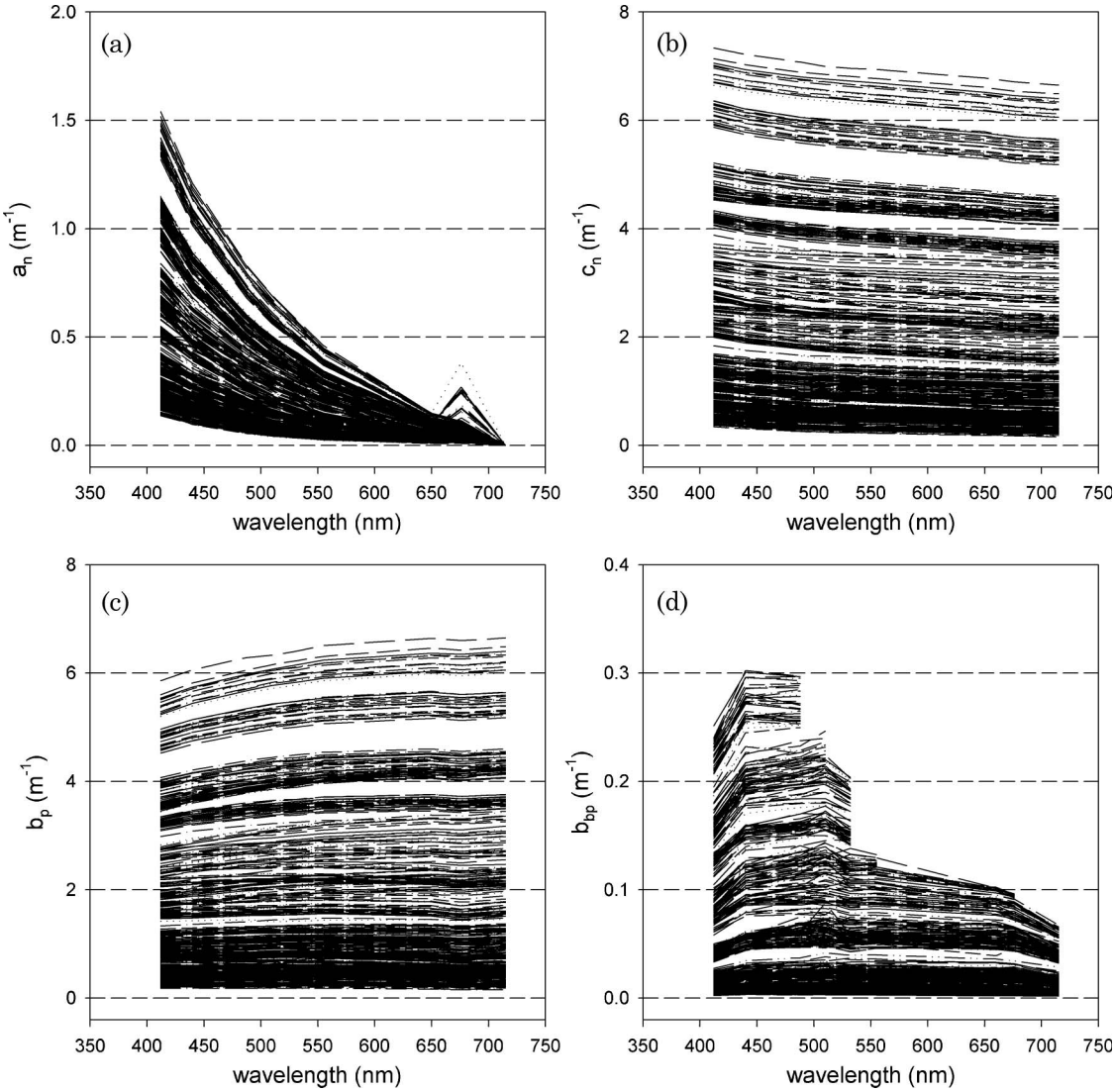

Fig. 2. IOP spectra for the full range of data collected in the Bristol Channel up to the point where all BB9 backscattering channels reached saturation. (a) Non-water absorption spectra increase strongly toward blue wavelengths, typical of strong mineral and/or CDOM absorption. Some stations show the influence of phytoplankton pigment absorption at 676 nm. (b), (c) Non-water attenuation and particulate scattering spectra show strong spectral consistency across the range of signals encountered. (d) Particulate backscattering spectra decrease toward both the blue- and red-NIR ends of the spectrum. Note that red-NIR channels reached saturation at much lower levels of turbidity than blue-green channels.

accounts for 96% of the observed variability and has a slope of 0.0479 with a 95% confidence interval of ± 0.0007. The best-fit offset (-0.0109) is both large and statistically significant. This is unexpected (zero values of b_{bp} and b_p ought to coincide) and indicates a systematic offset in the measurement data, either an underestimate of b_{bp} or an overestimate of b_p. Given that the calibration of the backscattering sensor

Table 1. Coefficients of Determination for Linear Regressions of IOPs against MSS and Chl

λ (nm)	b_{bp} Versus MSS	b_{bp} Versus Chl	b_p Versus MSS	b_p Versus Chl	a_n Versus MSS	a_n Versus Chl
412	0.8402	0.0049	0.8504	0.0044	0.8582	0.0081
440	0.8402	0.0057	0.8514	0.0039	0.8581	0.0095
488	0.8472	0.0088	0.8529	0.0038	0.8531	0.0085
510	0.8569	0.0092	0.8528	0.0040	0.8530	0.0061
532	0.8678	0.0017	0.8534	0.0040	0.8509	0.0049
555	0.7747	0.0072	0.8534	0.0039	0.8520	0.0045
650	0.7059	0.0518	0.8531	0.0031	0.8487	0.0478
676	0.7208	0.0493	0.8526	0.0025	0.6523	0.3063
715	0.6508	0.0611	0.8543	0.0035	-	-

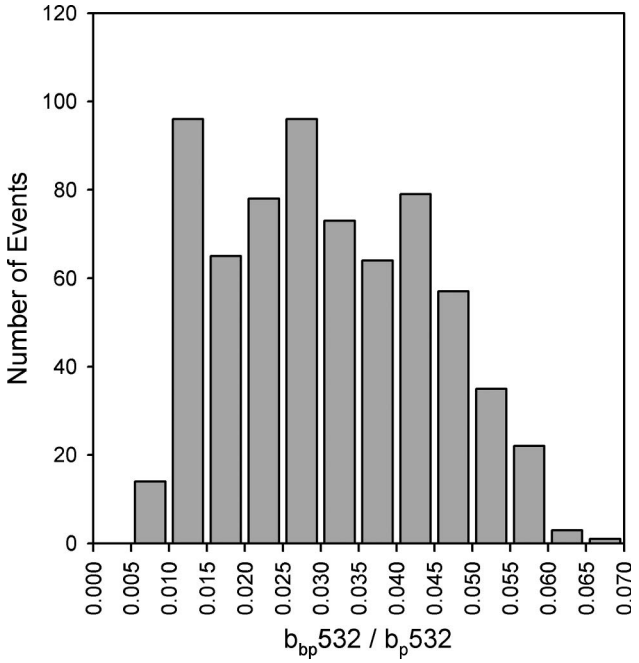

Fig. 3. Distribution of particulate backscattering ratios at 532 nm calculated on a point-by-point basis for Bristol Channel data shows an apparent order of magnitude variability.

determines a slope factor, it is difficult to see how this process could generate a systematic offset error. Furthermore, the AC9 calibration was performed to within the manufacturer's specified limits in our laboratory. One possible explanation is that the b_p values are overestimated as a result of the AC9 scattering correction, which assumes zero absorption at 715 nm. If this assumption is not valid in these waters [21], the absorption would be underestimated and, since $b_p = c_n - a_n$, scattering values would be overestimated. One advantage of the regression approach is that the slope of the best-fit line is unaffected by the presence of an offset error in either parameter, and represents an estimate of the best-fit b_{bp}/b_p for the entire population. Of course, the regression slope could still potentially be affected by errors in the calibration slope of the backscattering sensor, but a value of $b_{bp}/b_p = 0.0479$ is consistent with the presence of nonbiogenic mineral particles [15] and with previous values found in similar water types elsewhere in the Irish Sea [19].

Another potential benefit of the regression approach is the predictive power of the resulting best-fit parameters. Figure 4(b) shows that the mean point-by-point estimate of b_{bp}/b_p has poor predictive qualities, and that the apparent range of possible values suggested by the point-by-point range of b_{bp}/b_p strongly overstates the true variability observed in the overall population. This should be compared with the 95% prediction interval shown in Fig. 4(a), which gives a significantly better representation of where future measurements are expected to fall. It should be noted that these point-by-point values of b_{bp}/b_p are probably subject to underestimation due to the potential offset error in b_p. Offset correction of b_p and recalculation of b_{bp}/b_p results in a significantly modified distribution that is less skewed toward low values but retains a very broad range of values. The median of the distribution changes from 0.0294 to 0.0473, much closer to the best-fit regression value of 0.0479. These results emphasize the potential impact of offset errors on point-by-point estimates of b_{bp}/b_p, even though it has to be noted that errors in the calibration slope for b_{bp} measurements could cause significant differences for both point-by-point and regression estimates of b_{bp}/b_p.

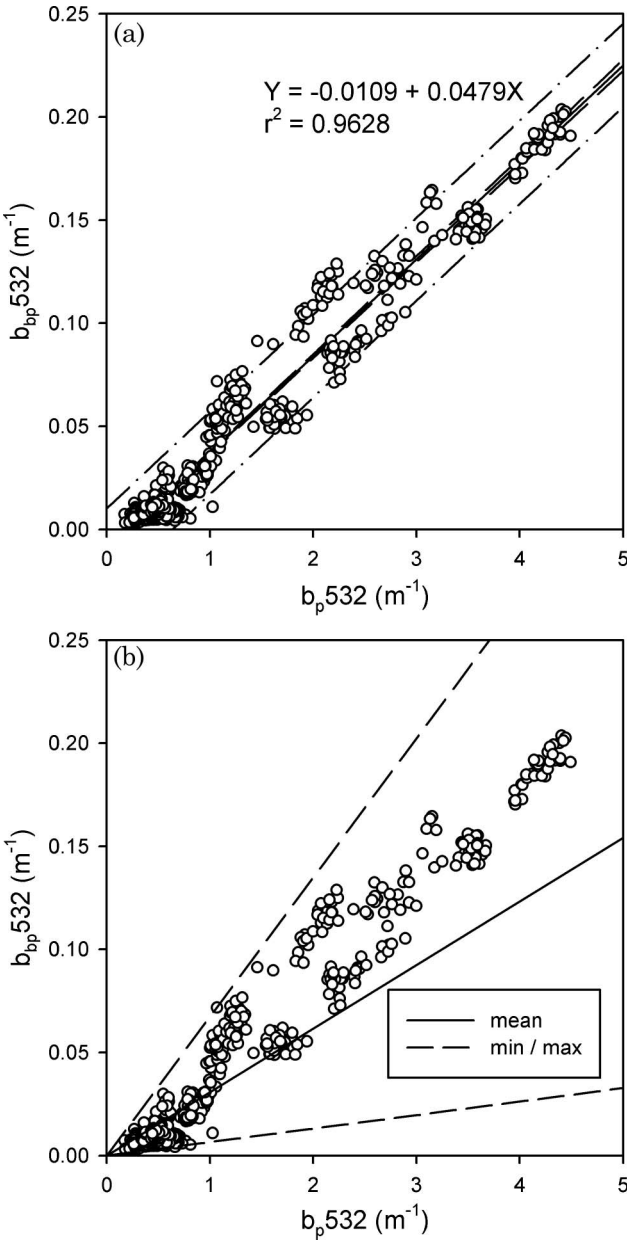

Fig. 4. Particulate backscattering plotted against particulate scattering with (a) best-fit regression (solid line), 95% confidence interval for the slope (dashed line) and 95% prediction interval (dashed-dotted line), and (b) point-by-point mean (solid line) and minimum/maximum range values (dashed lines).

E. Measurement Uncertainty and Apparent Point-by-Point Variability

Figure 4 demonstrated that the point-by-point approach significantly overstated the variability in b_{bp}/b_p for regional predictive purposes. One potential mechanism for the apparent variability given by the point-by-point approach is random measurement uncertainty in both b_{bp} and b_p. After all relevant corrections have been applied, the outputs from *in situ* instruments are measured values of scattering (b_{pm}) and backscattering (b_{bpm}). These differ from true values of b_p and b_{bp} through measurement uncertainties that we can call ε_{bp} and ε_{bbp}. As a result, the true particulate backscattering ratio is given by

$$\frac{b_{bp}}{b_p} = \frac{b_{bpm} \pm \varepsilon_{bbp}}{b_{pm} \pm \varepsilon_{bp}}. \quad (1)$$

If ε_{bp} and ε_{bbp} are small, b_{bpm}/b_{pm} will tend toward the true value. However, if measurement errors are significant, b_{bpm}/b_{pm} may deviate significantly from the true value. Manufacturers provide estimates of instrument noise that are related to electrical signal noise, optical detector noise, etc. However, when instruments are deployed in natural waters additional factors come into play (e.g., measurements are not made on identical sample volumes, there may be local heterogeneity of the sample, and pumping samples into the AC9 may cause aggregate disruption) so that the manufacturer's noise specifications for an individual channel are not necessarily relevant in this context. Instead, a measure of the overall random measurement uncertainty due to instrument noise combined with sample volume heterogeneity is required. One way to estimate this is to examine signals from two channels of the same instrument that are closely spaced spectrally. Assuming that wavelength dependence of b_p and b_{bp} for the population is small and reasonably uniform for a small wavelength difference, we can use residual analysis to estimate the combined measurement uncertainty of the b_p and b_{bp} signals.

Figure 5(a) shows particulate scattering at two wavelengths (510 and 532 nm) plotted against one another for the entire data set. The geometric mean regression line has a very small offset and a coefficient of determination almost equal to unity, suggesting that spectral variability between the two wavelengths for this population is well accounted for by the slope value of 1.0094. The corresponding plot of $b_{bp}532$ versus $b_{bp}510$ [Fig. 5(b)] demonstrates very similar characteristics, with the spectral variability between these two sets of measurements almost completely accounted for ($r^2 = 0.99$) by the geometric mean regression. Residual variability between each set of measurements can then be attributed to random measurement uncertainties. Figures 5(c) and 5(d) show residual b_p and b_{bp} values, obtained by subtracting values predicted from the regressions shown in Figs. 5(a) and 5(b), plotted against measured b_p and b_{bp}, respectively. These plots show that the measurement uncertainty range for each parameter does not increase significantly with increasing scattering signal, indicating that the range has a constant value, rather than a percentage or fractional figure. The magnitude of the range can be approximately estimated by taking the 95th percentile points of the absolute distribution, giving $\pm 0.009\ \mathrm{m}^{-1}$ for b_{bp} and $\pm 0.026\ \mathrm{m}^{-1}$ for b_p.

The fact that the measurement uncertainty range for each signal is constant, rather than proportional to the signal, is highly significant when we assess the source of apparent variability in the point-by-point backscattering ratio. In this analysis we take the best-fit relation between b_{bp} and b_p from Fig. 4(a), use it to correct measured b_p values by subtracting the observed offset ($0.0109/0.0479 = 0.2276$), and then calculate point-by-point b_{bp}/b_p values using the corrected b_p data. Figure 6 shows point-by-point b_{bp}/b_p plotted against b_p for the entire data set at 532 nm. Also shown is the best-fit estimate of b_{bp}/b_p ($= 0.0479$) from the regression in Fig. 4(a). It can be seen that the greatest apparent variability in point-by-point b_{bp}/b_p occurs for small b_p and that values tend toward the best-fit regression value when the scattering signal increases. We can now demonstrate that this behavior is directly attributable to random measurement uncertainties. Using Eq. (1) with values of b_{pm} from 0 to $5\ \mathrm{m}^{-1}$, corresponding predicted values of b_{bpm} obtained using the best-fit slope of 0.0479, and the uncertainty ranges for ε_{bp} and ε_{bbp} (± 0.026 and $\pm 0.009\ \mathrm{m}^{-1}$) found previously, it is possible to determine the bounds of parameter space that can be attributed to measurement uncertainties. These are shown as dashed curves in Fig. 6. A large number (>60%) of observations fall within these bounds, and the bounds increase in width rapidly as the scattering signals decrease. This is a direct consequence of constant values of ε_{bp} and ε_{bbp}. In effect, much of the apparent variability observed in point-by-point particulate backscattering ratios can be attributed to signal-to-noise issues becoming significant at low signal values.

F. Wavelength Dependence of the Particulate Backscattering Ratio

A previous study using a point-by-point approach and wavelengths between 442 and 620 nm found that spectral variability in mean values of b_{bp}/b_p was dwarfed by variability in the magnitude of the b_{bp}/b_p estimate at each wavelength [8]. This result can be reproduced with data from the Bristol Channel. Figure 7(a) shows mean values of b_{bp}/b_p, plotted as a function of wavelength, together with standard deviations and maximum/minimum range values. Using the point-by-point approach, there is appreciable spectral variability between blue- and red-NIR values, but it is largely within the bounds of the standard deviations of each measurement. Interestingly, Huot *et al.* [18] also show significantly lower b_{bp}/b_p at 650 nm compared to blue and green wavelengths using a point-by-point approach for data from very

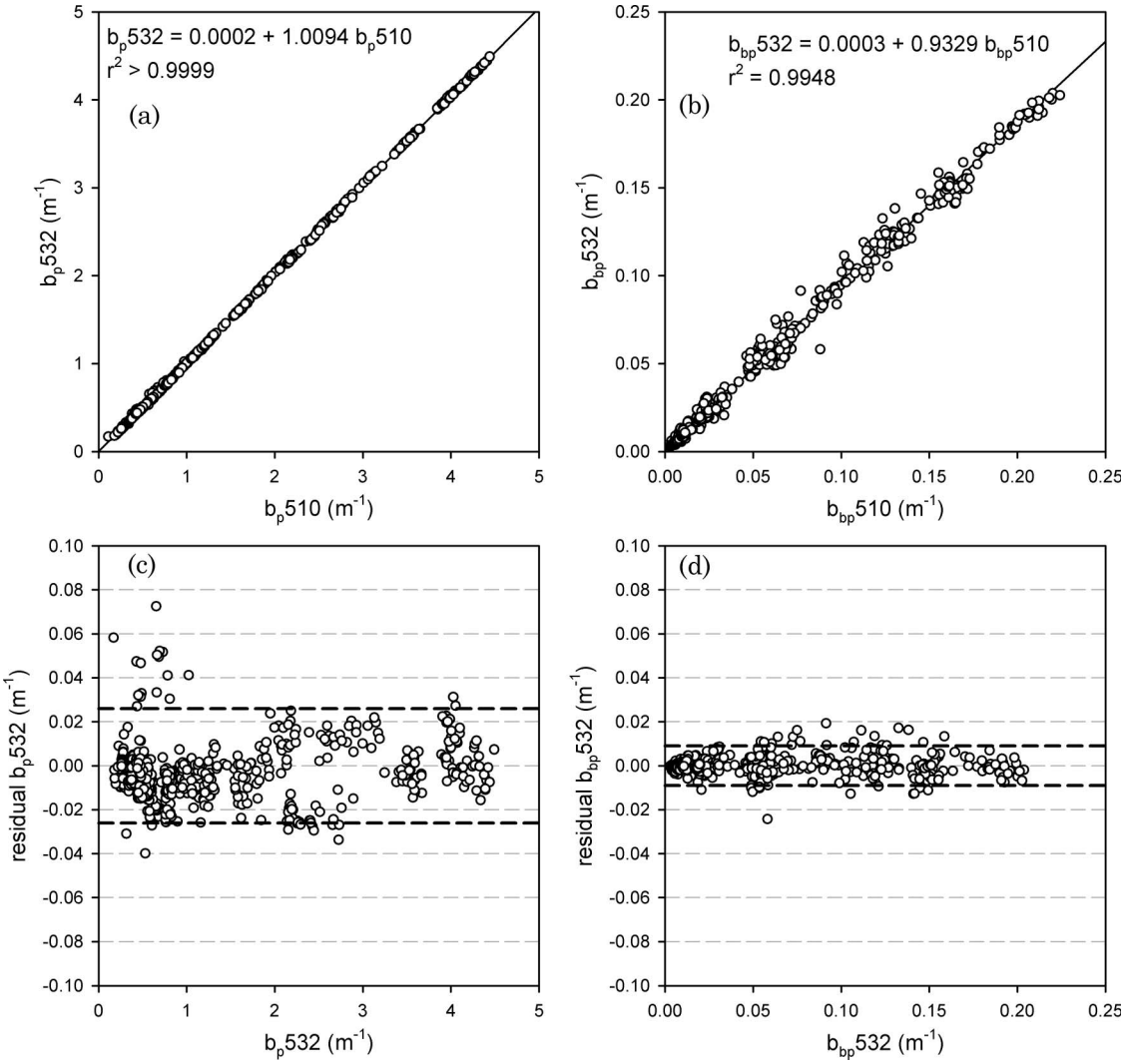

Fig. 5. Plots of (a) b_p532 versus b_p510 and (b) $b_{bp}532$ versus $b_{bp}510$ show that virtually all the spectral variability between these data sets can be accounted for with geometric mean regression best-fit lines. These regressions are used to derive residual values of (c) b_p532 and (d) $b_{bp}532$, which show that measurement uncertainty ranges are constant for each parameter.

clear South Pacific Ocean waters. Extension of the wavelength range out to the NIR does give a greater sense of wavelength dependency than both the Huot *et al.* [18] and Whitmire *et al.* [8] observations, but it would be difficult to justify a definitive conclusion of wavelength dependency taking this approach. However, performing geometric mean regressions in the same manner as Fig. 4(a) for each wavelength, and taking the best-fit slope as the best estimate of b_{bp}/b_p for the population, we obtain an alternative view of the spectral dependency of the particulate backscattering ratio. Figure 7(b) shows best-fit estimates of b_{bp}/b_p as a function of wavelength and associated 95% confidence intervals for the regression slopes. Coefficients of determination vary between 0.98 and 0.88 across the spectral range (decreasing with wavelength as scattering signals decrease) with offsets of the same magnitude and sign (−0.006 to −0.015) as the 532 nm value. These regression-based estimates of b_{bp}/b_p for the Bristol Channel data are generally higher than point-by-point mean values (which are potentially underestimated due to the offset error in b_p discussed earlier), but show a similar spectral dependence, with b_{bp}/b_p generally decreasing toward the red-NIR. The regression value of b_{bp}/b_p at 715 nm is ~57% of the value at 440 nm, representing a significant reduction in magnitude with wavelength. These values of b_{bp}/b_p are statistically significant, have good predictive power [Fig. 4(a)], and their wavelength dependence is consistent with previous results from similar waters elsewhere in the Irish Sea area [10]. Figure 7(b) also shows b_{bp}/b_p at 470 and 676 nm calculated using independent measurements of b_{bp} from a Hydroscat-2 instrument deployed at the same time as the BB9. The Hydroscat-2 observations confirm the magnitude of the BB9 signals (to within ~10%) and also the wavelength dependence. Correction for the effect of possible fluorescence contamination of the Hydroscat-2 676 nm channel would further reduce b_{bp}/b_p relative to the 470 nm channel. The fact that such similar results are obtained independently from two back-

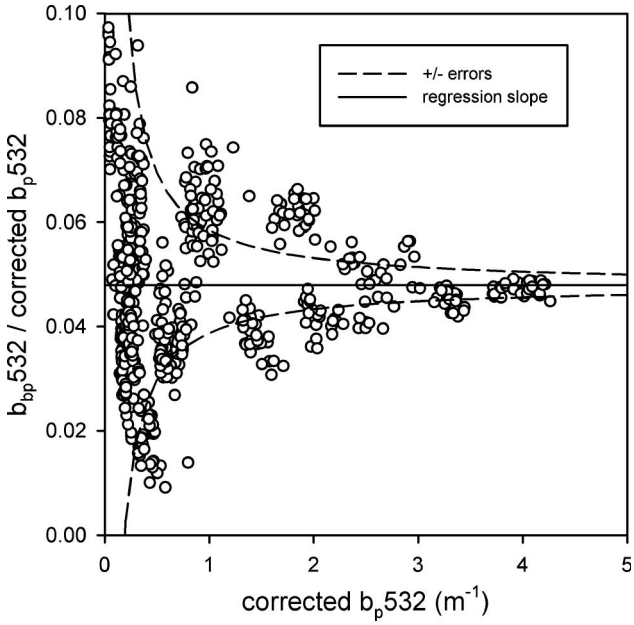

Fig. 6. Point-by-point values of b_{bp}/b_p calculated with offset-corrected b_p values show strong apparent variability at low scattering signals but tend toward the best-fit regression value of b_{bp}/b_p as scattering increases. More than 60% of observed point-by-point b_{bp}/b_p values fall within the region (dashed curves) that is accounted for by measurement uncertainties.

scattering meters calibrated by separate manufacturers using significantly different procedures provides a degree of confidence in our results. It is interesting to note that the discrepancy in our estimates of b_{bp}/b_p from the two different sets of instruments is rather close to the ~10% found by Boss *et al.* [14]. Thus the regression-derived values of b_{bp}/b_p suggest that the particle backscattering ratio is wavelength dependent for these mineral-rich waters. There remains the possibility, however, that our data could be affected by systematic biases in the calibration slopes of both of the backscattering sensors. Here we examine the magnitude of backscattering slope calibration error that would be required to maintain a spectrally flat model for b_{bp}/b_p. Figure 7(b) shows dotted curves corresponding to ±30% errors in the calibration slope for the BB9 and Hydroscat-2 sensors. This level of calibration slope error would be just sufficient to eliminate spectral dependency in b_{bp}/b_p. However, even with this magnitude of error in calibration slope (which is significantly greater than Whitmire *et al.* [8] predicted for the Hydroscat-2), we would require a systematic overestimate for blue-green wavelengths and an underestimate for red wavelengths that cannot readily be explained. Alternatively, the 715 nm channel of the BB9 sensor would have to underestimate b_{bp} by a factor of 0.6 in order to maintain a model of spectrally flat b_{bp}/b_p. We conclude that the field data indicate that the particulate backscattering ratio is wavelength dependent in the Bristol Channel unless there are significant undocumented uncertainties in the calibration of two widely used oceanographic backscattering sensors.

G. Relationship between Spectral Shape of b_{bp}/b_p and Particle Size Distribution

Morel and Bricaud [17] demonstrated that the particulate backscattering ratio depends on the real and

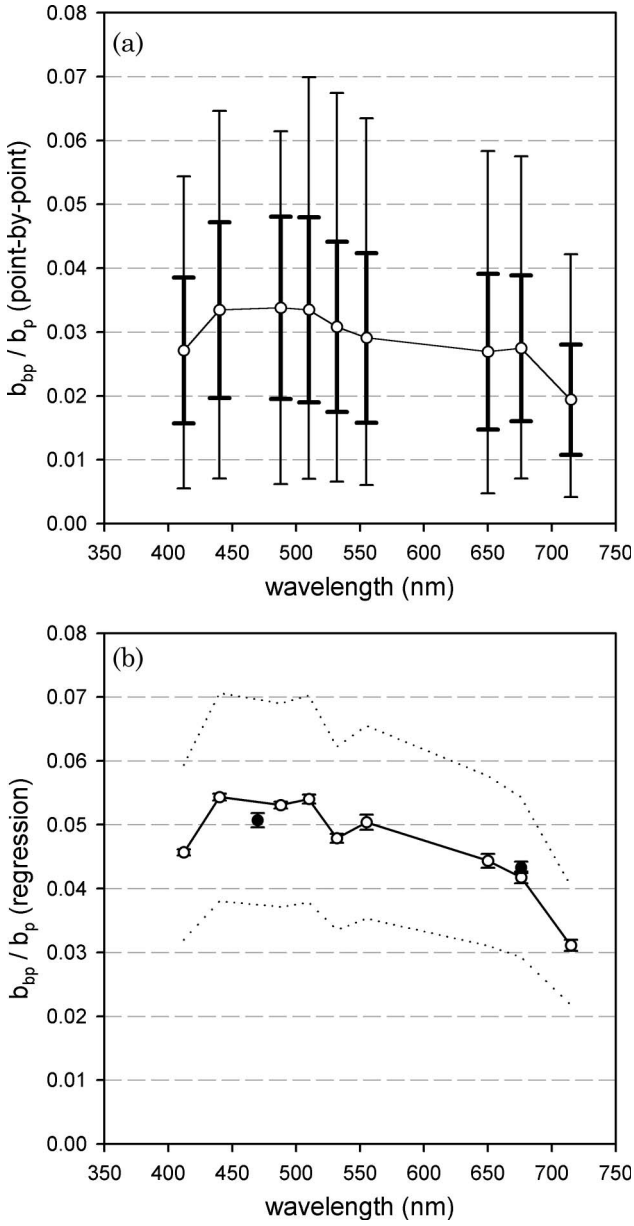

Fig. 7. (a) Wavelength dependence of point-by-point b_{bp}/b_p is insignificant compared to the apparent variability in magnitude at each wavelength. Standard deviations are shown with thicker error bars, maximum and minimum range values with thinner bars. (b) b_{bp}/b_p from regression slopes have tight confidence intervals and show potentially statistically significant wavelength dependency. b_{bp}/b_p calculated using Hydroscat-2 data (black circles) shows similar magnitude (±10%) and wavelength dependency. Dotted lines indicate intervals representing ±30% uncertainty in the slope calibration of the BB9. This is the minimum calibration slope error that could result in a spectrally flat particulate backscattering ratio.

imaginary components of the refractive index and the particle size distribution. Ulloa *et al.* [16] showed that assumptions of a power-law size distribution and negligible particle absorption generated spectrally flat particulate backscattering ratios, which is an attractive simplification for radiative transfer modeling. Given that our field data apparently diverge strongly from that scenario, it would be useful to consider what possible characteristics of natural particle populations could produce wavelength dependence in the particulate backscattering ratio. Consequently, Mie theory was used to calculate particulate backscattering ratio spectra for selected hypothetical particle size distributions and particle refractive indices to determine if our observations of wavelength-dependent b_{bp}/b_p are physically realistic. Calculations were performed for particle diameters from 0.01 to 100 μm and particulate backscattering ratios were calculated from

$$\frac{b_{bp}}{b_p} = \frac{\int_{\pi/2}^{\pi} \beta(\theta) \sin\theta \mathrm{d}\theta}{\int_{0}^{\pi} \beta(\theta) \sin\theta \mathrm{d}\theta}, \qquad (2)$$

where $\beta(\theta)$ is the VSF at scattering angle θ. Morel and Bricaud [17] showed that b_{bp}/b_p decreases with increasing absorption (and, hence, imaginary refractive index, n') for both monodispersed and polydispersed particle populations. The results of Ulloa *et al.* [16] suggested that the opposite is true for power-law particle size distributions (Ref. [15], Fig. 3), but this is not supported by results presented here. Babin *et al.* [26] suggested that the imaginary refractive index for mineral particles could be modeled so that n' increases exponentially with decreasing wavelength in a manner consistent with observed spectral absorption signals [Fig. 8(a)]. Figure 8(b) shows that increasing n' in the manner of Babin *et al.* [26] for mineral particles with an assumed real refractive index, $n = 1.15$ (relative to seawater), and a power-law size distribution with a slope factor, $\xi = 3$, results in a reduction in b_{bp}/b_p in the blue relative to the red. In contrast, our field data shows b_{bp}/b_p in the blue to be generally greater than at red wavelengths. Thus, although we cannot afford to ignore absorption effects, they are insufficient on their own to explain our observed spectral variability in b_{bp}/b_p.

Chami *et al.* [4] previously found that major angular features observed in spectral ratios of the VSF could only be accounted for by including both absorption effects and non-power-law size distributions in their Mie calculations. In order to observe the effect of varying particle size distribution in isolation, we set the imaginary refractive index to a constant value, $n' = 0.001$. Figure 9 shows hypothetical particle size distributions and corresponding b_{bp}/b_p spectra. Increasing the slope of a power-law particle size distribution increases the magnitude of b_{bp}/b_p but does not introduce any significant wavelength dependence, which is consistent with the results of Ulloa *et al.* [16]. However, introduction of an additional mode of particles, in this case a lognormal component

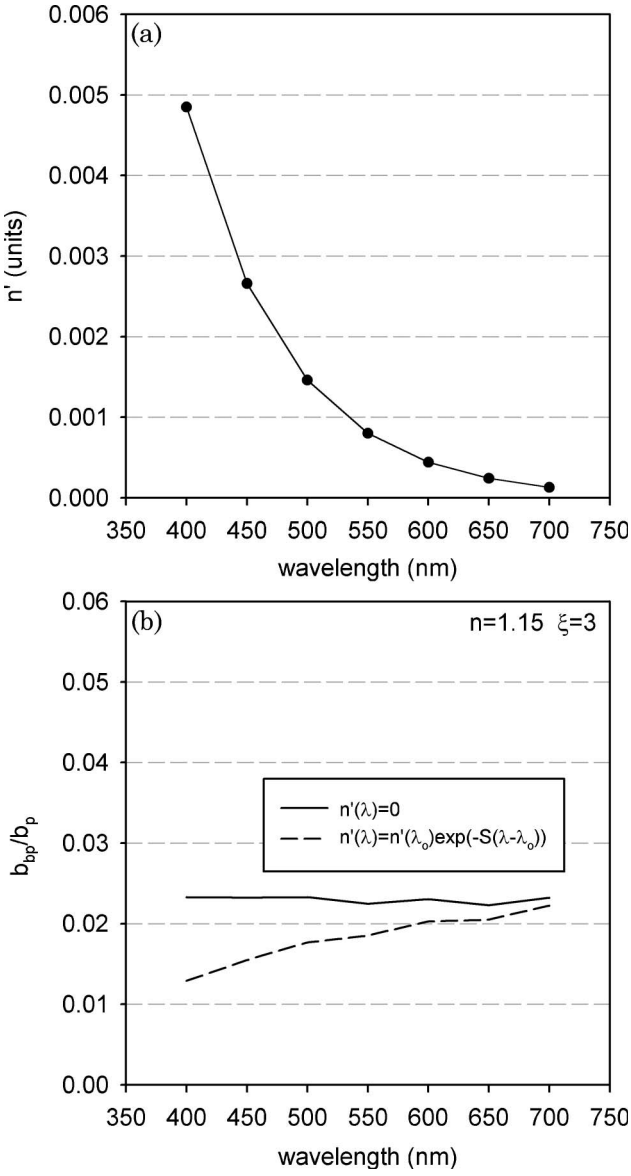

Fig. 8. Particulate backscattering spectra modeled using Mie theory with real refractive index $n = 1.15$ and a power-law size distribution with slope $\xi = 3$. (a) The imaginary refractive index is modeled to increase exponentially with decreasing wavelength in a manner consistent with observed mineral absorption characteristics. (b) The effect of mineral absorption is to depress b_{bp}/b_p in the blue (dashed curve) relative to the case with zero absorption (solid curve).

centered in the submicrometer diameter range [Fig. 9(b)], generates considerable wavelength variability in b_{bp}/b_p, which is more consistent with our field observations. These calculations are not presented as a fit to our data. We have not attempted to model likely spectral variability in the imaginary refractive index and would have too many unknown variables to be confident in any fit. Furthermore, Mie theory may not adequately describe the scattering properties of natural particles with a range of morphologies and shapes that might diverge more or less strongly from sphericity. However, Mie calculations serve to illustrate the fact that deviation from

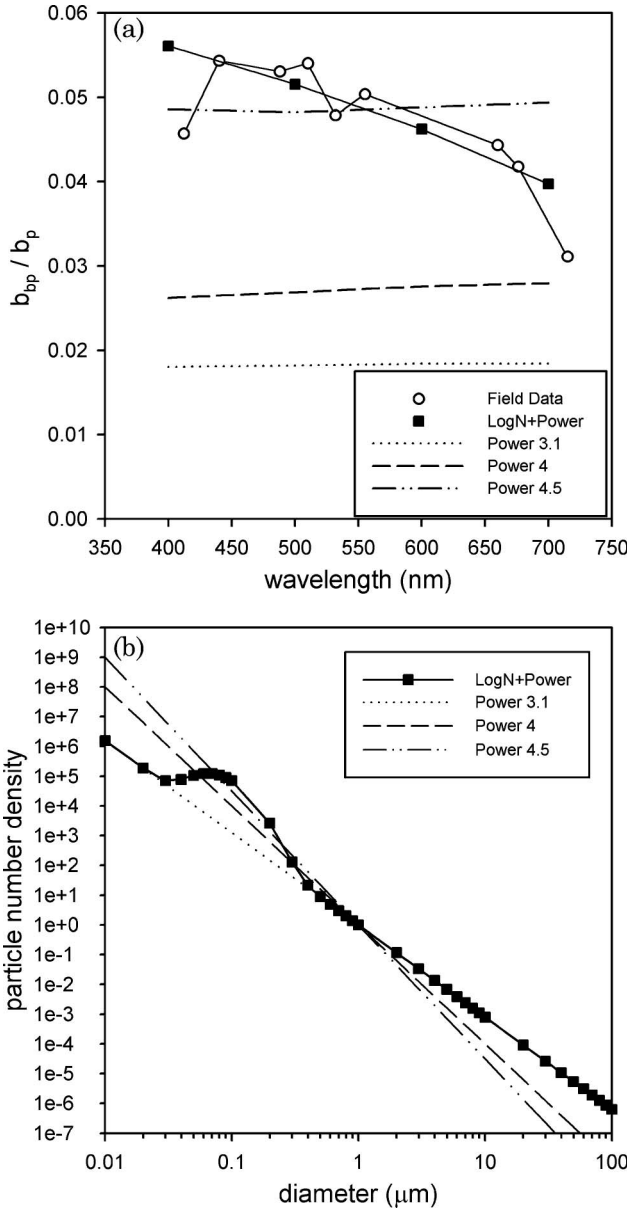

Fig. 9. Particulate backscattering spectra modeled by Mie theory for power-law size distributions with constant values of real and imaginary refractive index (dashed and dotted curves) exhibit no significant spectral variability. Introducing a separate mode (lognormal in this case) of particles is enough to introduce significant wavelength dependence in the b_{bp}/b_p spectrum (squares). b_{bp}/b_p from regression analysis of field data (circles) is shown for an order of magnitude comparison, but there are insufficient data available to perform a full theoretical validation of the field values of b_{bp}/b_p.

a power-law size distribution can introduce significant wavelength dependence in b_{bp}/b_p. In reality, the observed spectral variability in b_{bp}/b_p could be due to the combined effects of both particle absorption and deviation from a power-law size distribution. Furthermore, it is possible that natural particle size distributions may include subpopulations with different refractive indices. Risović [27] has examined the potential impact on the scattering properties of natural waters of multimodal, non-power-law PSDs with variable refractive indices for each component, and observed a degree of spectral variability in b_{bp}/b_p as a result of invoking a more complex particle size/refractive index model. The complexity of modeling such a system is beyond the scope of this paper, but it seems clear that our observation of wavelength-dependent b_{bp}/b_p is physically realistic if deviations from power-law size distribution and absorption effects are considered.

H. Inherent Optical Property Measurement Uncertainties

The ability to make *in situ* measurements of IOPs is a relatively recent advance and one that has yet to reach full maturity. A key step in this process is developing an understanding of random and systematic measurement uncertainties, assessing their magnitude, and working toward improved correction procedures. In this study we have seen evidence of both systematic errors (e.g., the offset between b_{bp} and b_p) and random measurement uncertainties. We have observed the impact that such measurement uncertainties can have on estimates of particulate backscattering ratio, particularly when the point-by-point approach is taken. It is essential that further efforts are made to understand measurement uncertainties in other optical water types. For example, the random uncertainty ranges observed for the tidally dynamic Bristol Channel may be larger than in oceanic waters where small-scale spatial variability may be less marked. This could explain why it is possible to make high-quality measurements in clear waters with essentially similar equipment to that used in this study [6,18,28].

I. Point-by-Point Versus Regression Approaches

This paper compared estimates of b_{bp}/b_p from point-by-point and regression analysis approaches and found that the point-by-point approach was highly sensitive to the effect of both random and systematic measurement uncertainties, particularly when scattering signals were low. Equation (1) gives a clear indication of why this is so. In this study, we were particularly fortunate to have measurements for waters with a strongly dominant class of particles generating a broad range of scattering magnitudes. This made it possible to successfully use geometric mean regression to determine an alternative estimate of b_{bp}/b_p for the population, which carries greater confidence because regression analysis weights random uncertainties against the whole signal range rather than individual signals, and the regression slope is independent of systematic offset errors. However, it should be noted that this approach does not resolve potential errors associated with the backscattering slope calibration and is only appropriate when a single population dominates and a reasonably broad range of signal magnitudes relative to the measurement uncertainty can be found.

J. Wavelength-Dependent b_{bp}/b_p and Particle Size Distribution

Spectral dependence in the particulate backscattering ratio is inconsistent with a power-law distribution of nonpigmented particles [16], and it is unlikely that inclusion of realistic wavelength-dependent imaginary refractive indices would be sufficient to produce a good fit with our field observations [4]. However, the introduction of additional modes of particles is sufficient to induce spectral variation in b_{bp}/b_p of the magnitude required to accommodate our results. Although we have insufficient data to fully model our observations using Mie theory, it is clear that the scope for understanding spectrally dependent b_{bp}/b_p is greatly increased if non-power-law particle size distributions and absorption effects are considered together, as previously suggested by Chami *et al.* [13]. It is equally important to realize the potential role of submicrometer particles in determining the backscattering properties of natural waters [29,30]. Peng and Effler [31] recently presented PSDs for minerogenic particles in a reservoir that deviated strongly from a power-law distribution, and Wells and Goldberg [32] used electron microscopy to show non-power-law distributions for colloidal particles for open waters, such as the South and North Atlantic oceans. Considerably more information about PSDs, including submicrometer particles, over broader geographic ranges than are currently available, is urgently required. The impact of non-power-law PSDs on scattering properties, particularly b_{bp}/b_p, should be studied in more detail as well, potentially using earlier work by Risović [27] as a starting point.

K. Optical Implications of Wavelength-Dependent b_{bp}/b_p

Developments in instrument technology are providing us with new opportunities to understand the complexity of natural particle assemblages and their optical properties. In a relatively short time we have moved from being reliant on a handful of *in situ* measurements [2] to a situation where the full VSF is being measured with specialist equipment in a variety of locations [3,4], and particulate scattering and backscattering data sets regularly consist of thousands of samples [7,8,18]. Variability in the magnitude of the particulate backscattering ratio has long been recognized, but it is now becoming clear that this may be coupled with spectral variability in some circumstances. It may be necessary in the future to include this variability in radiative transfer calculations, particularly when attempting to obtain closure with radiometric measurements. Significant spectral variability in b_{bp}/b_p, such as observed here, violates a key assumption in the Zaneveld *et al.* [20] scattering error correction procedure for AC9 measurements [10]. It also calls into question the validity of assumptions of power-law size distributions, and this has potential implications for estimating refractive index from scattering signals [14,15].

4. Conclusions

Our analysis suggests that random measurement uncertainties can play a major role in overstating variability in the magnitude of the particulate backscattering ratio. A key observation in this process is that the random measurement uncertainty range is constant, i.e., it does not scale with measurement signal and, as a result, signal-to-noise ratio deteriorates as signal levels drop. Random measurement uncertainties could have similar impacts on other important optical parameters involving ratios of IOPs, such as material-specific IOPs. One outcome from this work is a new question: how much of the observed variability in material-specific IOPs can be attributed to random measurement uncertainty? This will form the basis for future work on this topic, but it is already clear that we should not ignore IOP measurement uncertainties.

An original approach based on regression analysis has been used to parameterize measurement uncertainties and establish probable wavelength dependency in the particulate backscattering ratio for the mineral-rich waters sampled in this case study. Limitations in current sensor technology preclude a definitive statement for or against wavelength dependence of b_{bp}/b_p. Further work is needed to determine to what extent other natural waters exhibit significant wavelength dependence in b_{bp}/b_p. However, application of Mie theory to hypothetical PSDs has shown that wavelength dependency in b_{bp}/b_p can be generated by the effect of particle absorption (nonzero imaginary refractive index) on scattering and backscattering, and/or deviation of the PSD from a power-law distribution. One can envisage scenarios where these conditions could occur, such as resuspension of benthic material and the formation of algal blooms. Given the sensitivity of b_{bp}/b_p to submicrometer particles and the scarcity of PSD data available for this size class, there are reasonable grounds for wondering if wavelength-dependent scattering phase functions might be the norm rather than the exception in the global ocean.

References

1. T. J. Petzold, "Volume scattering functions for selected ocean waters," Tech. Rep. 72-28 (Scripps Institute of Oceanography, 1972).
2. X. Zhang, M. Lewis, M. Lee, B. Johnson, and G. Korotaev, "The volume scattering function of natural bubble populations," Limnol. Oceanogr. **47**, 1273–1282 (2002).
3. M. E. Lee and M. R. Lewis, "A new method for the measurement of the optical volume scattering function in the upper ocean," J. Atmos. Ocean. Technol. **20**, 563–571 (2003).
4. M. Chami, E. B. Shybanov, G. A. Khomenko, M. E.-G. Lee, O. V. Martynov, and G. K. Korotaev, "Spectral variation of the volume scattering function measured over the full range of scattering angles in a coastal environment," Appl. Opt. **45**, 3605–3619 (2006).
5. C. D. Mobley, L. K. Sundman, and E. Boss, "Phase function effects on oceanic light fields," Appl. Opt. **41**, 1035–1050 (2002).

6. M. S. Twardowski, H. Claustre, S. A. Freeman, D. Stramski, and Y. Huot, "Optical backscattering properties of the "clearest" natural waters," Biogeosci. **4**, 1041–1058 (2007).
7. W. A. Snyder, R. A. Arnone, C. O. Davis, W. Goode, R. W. Gould, S. Ladner, G. Lamela, W. J. Rhea, R. Stavn, M. Sydor, and A. Weidemann, "Optical scattering and backscattering by organic and inorganic particulates in U.S. coastal waters," Appl. Opt. **47**, 666–677 (2008).
8. A. L. Whitmire, E. Boss, T. J. Cowles, and W. S. Pegau, "Spectral variability of the particulate backscattering ratio," Opt. Express **15**, 7019–7031 (2007).
9. D. McKee, A. Cunningham, and S. Craig, "Semi-empirical correction algorithm for AC-9 measurements in a coccolithophore bloom," Appl. Opt. **42**, 4369–4374 (2003).
10. D. McKee and A. Cunningham, "Evidence for wavelength dependence of the scattering phase function and its implication for modeling radiance transfer in shelf seas," Appl. Opt. **44**, 126–135 (2005).
11. J. Piskozub, D. Stramski, E. Terrill, and W. K. Melville, "Influence of forward and multiple light scatter on the measurement of beam attenuation in highly scattering marine environments," Appl. Opt. **43**, 4723–4731 (2004).
12. D. Stramski and J. Piskozub, "Estimation of scattering error in spectrophotometric measurements of light absorption by aquatic particles from three-dimensional radiative transfer simulations," Appl. Opt. **42**, 3634–3646 (2003).
13. M. Chami, E. Marken, J. J. Stamnes, G. Khomenko, and G. Korotaev, "Variability of the relationship between the particulate backscattering coefficient and the volume scattering function measured at fixed angles," J. Geophys. Res. **111**, C05013 (2006).
14. E. Boss, W. S. Pegau, M. Lee, M. Twardowski, E. Shybanov, G. Korotaev, and F. Baratange, "Particulate backscattering ratio at LEO 15 and its use to study particle composition and distribution," J. Geophys. Res. **109**, C01014 (2004).
15. M. S. Twardowski, E. Boss, J. B. Macdonald, W. S. Pegau, A. H. Barnard, and J. R. V. Zaneveld, "A model for estimating bulk refractive index from the optical backscattering ratio and the implications for understanding particle composition in case I and case II waters," J. Geophys. Res. **106**, 14129–14142 (2001).
16. O. Ulloa, S. Sathyendranath, and T. Platt, "Effect of the particle size distribution on the backscattering ratio in seawater," Appl. Opt. **33**, 7070–7077 (1994).
17. A. Morel and A. Bricaud, "Theoretical results concerning the optics of phytoplankton, with special references to remote sensing applications," in *Oceanography from Space*, J. F. R. Gower, ed. (Plenum, 1981), pp. 313–327.
18. Y. Huot, A. Morel, M. S. Twardowski, D. Stramski, and R. A. Reynolds, "Particle optical backscattering along a chlorophyll gradient in the upper layer of the eastern South Pacific Ocean," Biogeosci. **5**, 495–507 (2008).
19. D. McKee and A. Cunningham, "Identification and characterisation of two optical water types in the Irish Sea from in situ inherent optical properties and seawater constituents," Estuar. Coast. Shelf Sci **68**, 305–316 (2006).
20. J. R. V. Zaneveld, J. C. Kitchen, and C. M. Moore, "The scattering error correction of reflecting-tube absorption meters," Proc. SPIE **2258**, 44–55 (1994).
21. D. Doxaran, M. Babin, and E. Leymarie, "Near-infrared light scattering by particles in coastal waters," Opt. Express **15**, 12834–12849 (2007).
22. J. M. Sullivan, M. S. Twardowski, J. R. V. Zaneveld, C. M. Moore, A. H. Barnard, P. L. Donaghay, and B. Rhoades, "Hyperspectral temperature and salt dependencies of absorption by water and heavy water in the 400–750 nm spectral range," Appl. Opt. **45**, 5294–5309 (2006).
23. E. Boss and W. S. Pegau, "Relationship of light scattering at an angle in the backward direction to the backscattering coefficient," Appl. Opt. **40**, 5503–5507 (2001).
24. R. A. Maffione and D. R. Dana, "Instruments and methods for measuring the backward-scattering coefficient of ocean waters," Appl. Opt. **36**, 6057–6067 (1997).
25. S. W. Jeffrey and G. F. Humphrey, "New spectrophotometric equations for determining chlorophylls a, b, c_1 and c_2 in higher plants, algae and natural phytoplankton," Biochem. Physiol. Pflanzen **167**, 191–194 (1975).
26. M. Babin, A. Morel, V. Fournier-Sicre, F. Fell, and D. Stramski, "Light scattering properties of marine particles in coastal and open ocean waters as related to the particle mass concentration," Limnol. Oceanogr. **48**, 843–859 (2003).
27. D. Risović, "Effect of suspended particulate-size distribution on the backscattering ratio in the remote sensing of seawater," Appl. Opt. **41**, 7092–7101 (2002).
28. D. Stramski, R. A. Reynolds, M. Babin, S. Kaczmarek, M. R. Lewis, R. Röttgers, A. Sciandra, M. Stramska, M. S. Twardowski, B. A. Franz, and H. Claustre, "Relationships between the surface concentration of particulate organic carbon and optical properties in the eastern South Pacific and eastern Atlantic Oceans," Biogeosci. **5**, 171–201 (2008).
29. D. Stramski and S. B. Wozniak, "On the role of colloidal particles in light scattering in the ocean," Limnol. Oceanogr. **50**, 1581–1591 (2005).
30. D. Stramski, E. Boss, D. Bogucki, and K. J. Voss, "The role of seawater constituents in light backscattering in the ocean," Prog. Oceanogr. **61**, 27–56 (2004).
31. F. Peng and S. W. Effler, "Suspended minerogenic particles in a reservoir: Light-scattering features from individual particle analysis," Limnol. Oceanogr. **52**, 204–216 (2007).
32. M. L. Wells and E. D. Goldberg, "The distribution of colloids in the North Atlantic and Southern Oceans," Limnol. Oceanogr. **39**, 286–302 (1994).